Effect of alumina source on ease of melting of glass batch

David A. Pierce, Pavel Hrma, José Marcial, Brian J. Riley, Michael J. Schweiger

Pacific Northwest National Laboratory, Richland, WA 99354

Abstract

The selection of raw materials affects the rate of batch-to-glass conversion. In all-electric melters, foam under the batch blanket limits the heat flux from the molten glass, thus slowing the rate of melting. Our study, in which we compare the melting behaviors of three batches formulated to vitrify high-alumina high-level waste, shows that a slowly dissolving refractory component can cause excessive foaming. Faster melting batches with gibbsite [$Al(OH)_3$] or boehmite [AlO(OH)] as an alumina source produced substantially less foaming than a batch with corundum (Al_2O_3). While gibbsite and boehmite dissolved below 500°C, corundum was still present in the batch up to 900°C; hence, the glass-forming melt lacked alumina in the batch with corundum. The low viscosity of that batch caused the open pores to close prematurely at 660°C, trapping gases and expanding to foam. This would explain the literature-reported slow melting rate of a batch with corundum, as compared to batches with gibbsite and boehmite.

Introduction[1]

Our study was motivated by the effect of alumina source on the rate of melting observed in [1], a publicly available report that provides a summary of studies of the effects of composition on the rate of

[1] This work was supported by the U.S. Department of Energy Federal Project Office Engineering Division for the Hanford Tank Waste Treatment and Immobilization Plant.

melting in continuous electric melters of various scales conducted to assess the performance of the Hanford Waste Treatment and Immobilization Plant currently under construction in Washington State. For information regarding nuclear waste vitrification, we refer the reader to the review by Vienna [2] and the literature cited there.

Generally, the selection of batch materials affects the rate of glass melting. In particular, additions of refractory components, such as crystalline alumina (corundum) [1], zinc oxide [3], or zirconia (baddeleyite) decrease the rate of melting of glass batches in continuous melters. This effect can be considerable. Table 1 lists the results of melter experiments with three batches reported in [1]. These batches were formulated to vitrify a simulated high-alumina high-level waste and each was prepared with a different alumina precursor: one with gibbsite [$Al(OH)_3$], another with boehmite [$AlO(OH)$], and the other with corundum (Al_2O_3). Table 1 shows that batches with gibbsite and boehmite melted substantially faster than the batch prepared with corundum.

The list of alumina sources used for commercial glasses is extensive [4]. In nuclear waste glasses, alumina can be a waste component, typically in the form of gibbsite and boehmite, or a glass-forming additive. Whereas alumina rarely is a major component in commercial glasses, nuclear waste glass can contain up to 30 mass % of alumina [5].

The considerable effect of batch materials on the rate of melting has important economic consequences. The life cycle of high-level waste vitrification at Hanford depends on the rate of melting, and thus will be affected by the selection of glass-forming and modifying additives used for waste vitrification. Additionally, the chemical and mineralogical form of waste simulants influences prediction of the performance of waste-glass melters. Thus, corundum appears a poor substitute for gibbsite and boehmite, which are common in Hanford high-level wastes.

The very fact that the corundum, or any refractory oxide, slows down the melting of glass is intriguing because it can hardly be attributed to the refractoriness alone if the residence time of glass in the melter is long enough to allow a refractory oxide to dissolve and homogenize.

In an all-electric melter, the rate of melting of the batch blanket, or the cold cap, is determined by the heat flux delivered to the cold cap from the pool of molten glass on which the cold cap floats. Accordingly, the presence of a refractory oxide, such as corundum, must affect the heat transfer to or within the cold cap.

Indeed, laboratory examination revealed that the batches with corundum produced copious foam whereas the batches with gibbsite did not [6, 7]. Foam accumulated under the cold cap insulates the cold cap from the melt, thus reducing the heat flow to the cold cap [8-11]. The intriguing question is about the mechanism by which corundum, a stable oxide that does not participate in any gas-evolving reaction, intensifies foam accumulation.

Two types of foam are associated with glass melting. Primary foam, term coined by Gerrard and Smith [12], is batch expansion caused by the evolution of batch-reaction gases, such as CO_2, after enough glass-forming melt was produced in the batch to close the open pores. Secondary foam is generally a term reserved for foam created in molten glass from fining-reaction gases [12, 13]. In high-level-waste glass melts, secondary foam results from oxidation-reduction reactions, mainly involving ferric oxide. Neither foam is directly associated with the dissolution of corundum in molten glass.

This study employs several experimental techniques to compare the melting behavior of three high-alumina batches with identical compositions except for sources of alumina. It is focused on the difference between batches containing corundum and gibbsite, although experiments were also performed with a batch containing boehmite. As argued in the Discussion section, excessive foaming of the corundum-containing batch can be attributed to the early closure of open pores caused by the low viscosity of the glass-forming melt.

Experimental Approach

Table 2 shows the composition of a batch used in previous studies [10, 14] with gibbsite, $Al(OH)_3$ (Almatis, Lot No. 0724131923), as the alumina source. The other two batches examined in this study contained equivalent fractions (g per g glass) of corundum (Sigma-Aldrich®, Lot No. 342688) and boehmite (Nabaltec, Lot No. 047235), i.e., 0.240 of Al_2O_3 and 0.280 of AlO(OH). Fractions of all other components remained identical. All batches were made with quartz particles of 75 µm as the source of silica. The particle size of corundum, by image analysis, was 45.6 ± 8.6 µm. The glass composition, in terms of targeted mass fractions, was SiO_2 (0.305), Al_2O_3 (0.240), B_2O_3 (0.152), Na_2O (0.096), CaO (0.061), Fe_2O_3 (0.059), Li_2O (0.036), Bi_2O_3 (0.011), P_2O_5 (0.011), F (0.007), Cr_2O_3 (0.005), PbO (0.004), NiO (0.004), ZrO_2 (0.004), SO_3 (0.002), K_2O (0.001), MgO (0.001), and ZnO (0.001). As described elsewhere [14], batches were prepared as slurry and were dried at 105°C overnight in an oven.

To measure the expansion of a batch during heating, ~1.5 g of batch was pressed at ~7 MPa into a cylindrical pellet ~13 mm in diameter and ~6.5 mm high. Each pellet was placed into a Deltech© (Denver, CO, U.S.A) furnace with a silica-glass viewing window and heated at 5°C/min on an alumina plate to 1000°C. Pellets were photographed at regular intervals, and their profile areas were measured with Photoshop® (Adobe®, San Jose, CA, U.S.A.). Next to the pellet was a Pt wire, 10-mm in length, which was used as a scale gauge. The profile area, A, was normalized to the profile area of a hemispherical body of the glass, i.e., to $A_g = (9\pi/32)^{1/3}(m_p/f\rho_g)^{2/3} = 0.9596(m_p/f\rho_g)^{2/3}$, where m_p is the initial pellet mass, f is the batch mass fraction per glass, and ρ_g is the glass density.

For X-ray diffraction (XRD) and microscopy examinations, approximately 10-g samples were heated at 5°C/min to temperatures of 400 to 1200°C in either a porcelain crucible (samples heated to ≤700°C) or Pt/10%Rh crucibles (samples heated to 800 to 1200°C) and air quenched. Each sample was weighed before and after the heat treatment. Half of the specimens were powdered and mixed with

~5 mass% CaF_2 as an internal standard for XRD. The other half of specimens, heat treated to 1100 and 1200°C, were used to make thin sections for optical microscopy.

XRD was performed with a Bruker® D8 Advance diffractometer (Bruker AXS Inc., Madison, WI) equipped with a Cu Kα target at a power level of 40 kV and 40 mA. The instrument utilized a LynxEye™ position-sensitive detector with an angular range of 3° 2θ. The mass fractions of crystalline phases were obtained from XRD patterns with Jade® and RIQAS® software (MDI, Livermore, CA, U.S.A.).

Optical microscopy on samples heat-treated to 800 to 1200°C was performed with Olympus® (Center Valley, PA, U.S.A.) SZH10 and PMG-3 microscopes. Samples of batches containing corundum and gibbsite, heated to 600 and 700°C, were viewed with a JEOL© (Akishima, Tokyo, Japan) 5900 scanning electron microscope (SEM) and analyzed with an EDAX© (Mahwah, NJ, U.S.A.) lithium-drifted silicon energy-dispersive X-ray spectrometer (EDS). Since the samples were not fully sintered, they were cast in an epoxy resin and polished to an optical quality finish before analysis.

Finally, batch samples, ~20 to 50 mg, were analyzed with TA Instruments'© (New Castle, DE, U.S.A.) SDT Q-600 for thermo-gravimetric analysis (TGA).

Results

From TGA, the total mass losses on melting were ~0.27 g/g glass for the gibbsite batch, ~0.17 g/g glass for the boehmite batch, and ~0.15 g/g glass for the corundum batch, roughly corresponding to the different content of water in the alumina sources, but were slightly smaller than those obtained from the stoichiometry of the batched chemicals—see Table 3. As seen in Figure 1, the peak heights and positions in the TGA plots reveal large differences in gas-releasing reactions between batches that differ solely in the alumina source. Further investigation of these reactions and associated off-gas is presently underway.

Figure 2 displays photographs of the cylindrical pellets taken at specific temperatures and Figure 3 shows the plots of the normalized profile area, A/A_g, against temperature. After mild gradual expansion, the batch with corundum shrank starting at ~600°C, reached a minimum profile area at ~650°C, and then rapidly expanded to more than twice the minimum profile area at ~850°C (see also shrinking and expansion of pellets in Figure 2). Unlike the pellet with corundum, the pellet from the batch with gibbsite maintained a nearly constant profile area until it shrank at ~700°C, reaching a minimum profile area at ~800°C. The pellet profile area then began to increase, becoming ~40% larger at ~950°C than the minimum profile area. The pellet from the batch with boehmite responded to heating similarly to the batch with gibbsite except that both the minimum and maximum profile areas occurred at ~50°C lower temperatures. All pellets finally collapsed to a bubbly glass that spread over the alumina support plate.

Figure 4 shows the undissolved quartz and corundum fractions versus temperature, in which arctangent trend lines were fitted to the data. A notable difference in the extent of quartz dissolution can first be seen at ~400°C where the batch containing corundum has lost ~20% of the initial quartz while batches with gibbsite and boehmite lost <10%. The first derivatives of the arctangent trend lines, Figure 5, show that the temperature of the maximum rate of quartz dissolution increased in the order corundum-gibbsite-boehmite; the maximum rate of dissolution also slightly increased in that order, just enough for the quartz to be fully dissolved at around the same temperature in all batches.

Corundum dissolved rapidly between 700 and 1000°C. Hence, corundum had remained inert up to ~700°C. In contrast with corundum, gibbsite and boehmite could not be detected by XRD (Figure 6) even at temperatures as low as 500°C. Boehmite was only detected at temperatures ≤ 400°C in both gibbsite and boehmite batches. Immediately after the boehmite disappeared at 500°C, nepheline was produced and existed up to 900°C in the feed with gibbsite, and up to 800°C in the feed with boehmite.

Sodalite was produced in batches within the range of 500°C (600°C in the feed with corundum) to 1000°C. In all three batches, hematite was present up to ~1000°C whereas spinel formed at 900°C.

Quartz and corundum particles can be seen in SEM micrographs, Figure 7. At 600°C, the corundum particles are seen in region b of Figures 7A and 7B. Grayish regions, (a in Figures 7A and B, and c and d in Figure 7C) are rich in Fe_2O_3. The round dark object, region a, Figure 7C (the gibbsite batch, 700°C), is a quartz particle surrounded by a thin diffusion layer.

Optical micrographs, Figure 8, show sections of melts from batches with corundum and gibbsite heated to 1100 and 1200°C. At 1100°C, the melts somewhat differ in the size and distribution of bubbles and appear fairly similar in homogeneity. Dark regions contain tiny crystals of spinel (magnetite). At 1200°C, all bubbles are gone and the crystals are nearly uniformly distributed within each melt.

Discussion

The alumina source substantially influences batch behavior throughout the whole temperature interval of the batch-to-glass conversion, including the early stages. Reactions between waste components and additives occur as soon as they are mixed in the slurry and then during drying, as the differences between as-batched and dried masses, listed in Table 3, indicate. These reactions include those between acids and bases (NaOH and H_3BO_3), formation of solid solutions of salts, and interactions of aluminum hydroxide and oxyhydrate with dissolved components. However, the important differences between the behaviors of batches with gibbsite or boehmite and that of the batch with corundum occur during the heat treatment. These differences influence the initial gas-evolving reactions (Figure 1), the kinetics of quartz dissolution (Figures 4 and 5), the volume expansion or foaming (Figures 2 and 3), and the formation and motions of bubbles (Figure 8).

The initial gas-evolving reactions and the kinetics of quartz dissolution are related through the generation of glass-forming melt in a process that influences volume expansion (foaming) [10, 14, 15, 16]. The initial reactions evolve the chemically bonded water from salts, hydroxides, oxyhydrates, and acids. Nearly simultaneously with these reactions, the oxyionic salts produce eutectic melts, the borates generate the first glass-forming melt, and the hydroxides and oxyhydrates become amorphous oxides, mainly Al_2O_3, but also a portion of Fe_2O_3 (the other portion becomes hematite). Amorphous oxides, in turn, dissolve in both molten salts and molten borates. The addition of Al_2O_3 to the borate melt considerably increases its viscosity [17].

The batch melting reactions are numerous and complex. Therefore, it is difficult to identify the chemistry of various overlapping TGA peaks seen in Fig. 1. By stoichiometry, the gases released by early reactions from the gibbsite-containing batch (Table 1) are H_2O (1.20×10^3), CO_2 (94), NO (14), and O_2 (9); the numbers in parentheses show m^3 of gas per kg of glass at 630°C. Most of these gases are released from reactions between components rather than by simple decomposition of hydroxides and salts. The peak at ~130°C in the corundum-containing batch can possibly be attributed to borax, a reaction product of NaOH and H_3BO_3; the peak is missing in the other two batches, where NaOH had possibly reacted with gibbsite and boehmite to form sodium aluminate.

Both melts, ionic and covalent, attack quartz particles [16]. Alkali nitrates and carbonates react with quartz to form alkali silicates that fuse with the borate melt. While the borate melt dissolves quartz directly, it also protects it from molten salts. The alumino-borate melt occupies more space (there is 24 mass% Al_2O_3 in the final glass) and is more viscous, hence less aggressive, than the melt without alumina in the corundum-containing batch. This may explain why <10% of quartz was dissolved in the batches containing gibbsite or boehmite at 400°C, whereas more than twice as much quartz was dissolved in the batch containing corundum.

As we argue below, a lower viscosity of the glass-forming melt in the corundum-containing batch may also be responsible for the earlier closure of pores, i.e., the lower temperature at which the batch

volume reaches a minimum. The rapid expansion that follows the minimum volume indicates that the glass-forming melt has become connected, i.e., the open porosity, through which evolving gases were escaping freely to the atmosphere, has closed. The connected melt presents a barrier to gases trapped in bubbles, which cannot escape because the melt viscosity is high. If the porosity becomes closed at a temperature at which the batch gases are still evolving, the growing bubbles change the bubbly melt into primary foam. Primary foam expands to cellular foam and eventually collapses internally into large cavities that burst into the atmosphere because of the increasing internal pressure and decreasing melt viscosity as the temperature continues to increase [10, 15].

The temperature at which the glass-forming melt becomes connected determines whether primary foam will occur in the batch. The batch with corundum shrank to a minimum volume—the point at which glass melt became connected—at a temperature of 660°C, whereas the batch with boehmite reached the minimum volume at 750°C and the batch with gibbsite at 810°C (Figure 3). In borosilicate waste glasses, the gas-evolving batch reactions are complete by 700 to 800°C, typically by 750°C [18-20]. The crucial point is that if the melt from the batch with corundum became connected while batch gases were still evolving, copious primary foam was the result; whereas the melts from the batches with gibbsite and boehmite released the batch gases without producing primary foam.

As hinted above, the cause of the early closure of open porosity in the batch with corundum appears associated with the delayed incorporation of alumina into the glass-forming melt. Factors that influence the temperature at which the glass-forming melt becomes connected are the volume fraction of the melt (the melt-solid ratio) and the viscosity [10]—a tricky concept because the melt is far from homogeneous at this stage. We can assume that in the batches with gibbsite and boehmite, the melt with a higher alumina content, though with a somewhat lower silica content, had a higher viscosity, and thus moved more slowly, allowing the pores to close at a higher temperature.

The other source of bubbles, the redox or fining reactions (and also the decomposition of sodalite—see Figure 6), produce secondary foam, to which the volume expansion in batches with gibbsite and boehmite can solely be attributed. In the melt from the batch with corundum, secondary foam was

produced before primary foam could collapse. Thus, in the batch with corundum, the transition from primary foam to secondary foam was continuous.

Though expansion from primary foam in the melt can be avoided by an appropriate choice of the chemical form of batch components, the presence of secondary foam is inevitable. In the glass melts under study, secondary foam results from oxidation-reduction reactions, mainly involving ferric oxide [21]. These reactions are initially suppressed by nitrates, which are strong oxidizing agents. After nitrates are gone above 750°C, redox reactions reach equilibrium with oxygen in bubbles. The oxidation-reduction equilibria depend on the temperature and the melt basicity. As temperature increases, the equilibria shift to the reduced state and oxygen is liberated. Silica from dissolving quartz decreases melt basicity [22], thus contributing to the secondary foam development by shifting iron redox equilibria in the direction of oxygen release.

Other contributing factors are dissolution and precipitation of iron-containing crystalline phases. As has been suggested by Henager et al. [15], the dissolving hematite and the precipitating spinel may help accelerate the evolution of oxygen from the redox reaction $2\ Fe_2O_3(m) \rightarrow 4\ FeO(m) + O_2(g)$, where *m* and *g* denote the melt and gas phase, respectively. Dissolving hematite supplies Fe_2O_3 to the melt by the reaction $Fe_2O_3(c) \rightarrow Fe_2O_3(m)$, where *c* denotes the crystalline phase. At the same time, FeO reacts with Fe_2O_3, precipitating magnetite by the reaction $FeO(m) + Fe_2O_3(m) \rightarrow Fe_3O_4(c)$, which removes FeO from the melt. Both reactions, dissolving hematite and precipitating magnetite, shift the oxidation-reduction reaction to the right, thus promoting oxygen evolution, and consequently secondary foaming.

The fact that the slow-melting batch with corundum (see Table 1) generated massive primary foam, whereas the faster-melting batches with gibbsite did not, indicates that primary foam is likely a major cause of slow melting of glass batches. Secondary foam is less detrimental because it can be swept away by convection currents, especially by forced convection (bubbling), from the cold cap bottom to the free surface of the melt, where it can collapse or accumulate. The faster melting of the batch with

boehmite as compared to that with gibbsite remains unexplained. Attributing it to the smaller content of water in boehmite seems somewhat speculative.

The differences in amounts and sizes of bubbles between the melts at 1100°C (Figure 8) are probably associated with the melt homogeneity. In a less homogeneous melt, bubbles pass through less viscous portions that are likely to be connected, because high-viscosity inhomogeneities surround the dissolving silica and alumina grains. This may account for the presence of large bubbles in the melt from the batch with gibbsite. Photographs of samples taken at 1200°C indicate that melts from all three batches were nearly equally homogeneous at this temperature. The streaks, barely visible in the images, were caused by convection. Two sources of natural convection operate in crucible melts. Convection driven by surface tension gradients results from Na_2O and B_2O_3 volatilization in the meniscus area. These currents bring the melt to the surface where the ferrous-ferric ratio is altered by the diffusion of oxygen from the melt to the atmosphere, resulting in a change of phase equilibria between the melt and submicron iron-containing crystals (mostly magnetite). This change is reflected in the change of color that makes the streaks visible. The other source of streaks is associated with silica-rich inhomogeneities stuck to the crucible bottom. These inhomogeneities, some containing residues of quartz particles, have high viscosity and do not contain spinel crystals, which makes them transparent. Gas bubbles nucleate around them and drag the inhomogeneities upward to the melt surface. A typical example of this effect is shown in Figure 9.

The results of this study support our initial hypothesis that the slow melting of the batch with corundum is caused by foam generation. Nevertheless, the batch-to-glass conversion process described in this section, though plausible, is hypothetical in various aspects. Hopefully, it will inspire research into diffusion processes that occur in the glass-forming melt. From a technological point of view, the set of simple tests used in this study may allow preselecting batches for conducting more expensive scaling-up experiments.

Conclusion

The alumina source in otherwise identical glass batches affects the reaction sequence during melting, the kinetics of quartz dissolution, and, most notably, the batch expansion. The batch with corundum exhibited ample primary foam, which was absent in batches prepared with gibbsite and boehmite. Excessive foaming of the batch with corundum was most likely caused by an early closure of open pores by the glass-forming melt that had a low viscosity because most of the alumina was still undissolved when the pores were closing. The lower production rate when a batch containing corundum was processed in a continuous electric melter can thus be attributed to the extensive foaming caused by the late incorporation of alumina into the glass-forming melt.

Acknowledgements

The authors are grateful to Albert Kruger for his assistance and guidance and to Dong-Sang Kim for his help and insight in weekly meetings as well as Mark Steward for his contributions. Pacific Northwest National Laboratory is operated for the U.S. Department of Energy by Battelle under Contract DE-AC05-76RL01830.

References

1. K. S Matlack., H. Gan, M. Chaudhuri, W. Kot, W Gong, T. Bardakci, I. Pegg, and J. Innocent, *DM100 and DM1200 melter testing with high waste loading glass formulations for Hanford high-aluminum HLW streams*, VSL-10R1690-1, Vitreous State Laboratory, Washington DC, 2010.

2. J. D. Vienna, Nuclear waste vitrification in the United States: Recent developments and future options, *Int. J. Appl. Glass Sci*. 1 [3] 309-321 (2010).
3. H. H. Russell III, W. R. Ott, "The effect of batch preparation on some zinc opal glasses," *Glass Technol*. 21, 237-243 (1980).
4. F. V. Tooley, *The handbook of glass manufacture*, Vol. I, p. 24, Books for Industry, New York, 1974.
5. J. D. Vienna, A. Fluegel, D. S. Kim, P. Hrma, *Glass Property Data and Models for Estimating High-Level Waste Glass Volume*, PNNL-18501, Pacific Northwest National Laboratory, Richland, Washington, 2009.
6. P. Hrma., M. J. Schweiger, C. J. Humrickhouse, J. A. Moody, R. M. Tate, N. E. TeGrotenhuis, B. M. Arrigoni, and C. P. Rodriguez, "Effect of melter-feed-makeup on vitrification process," *2009ISRSM, Proceedings of International Symposium on Radiation Safety Management*, Daejeon, Korea, 280-290, 2009.
7. D. A. Pierce, P. Hrma, and M. J. Schweiger, "Effect of alumina source on HLW–feed melting process," *Proceedings of Materials Science and Technology 112th Ann. Meeting*, CD-ROM, Amer. Ceram. Soc. and ASM Intern. 2010.
8. P. Hrma, "Melting of foaming batches: nuclear waste glass," *Glastech. Ber*. **63K**, 360-369 (1990).
9. J. Kloužek, M. Arkosinová, L. Němec, and P. Cinibusová "The Role of Sulphur Compounds in Glass Melting," *Eur. J. Glass Sci. Technol.* A **48**, 176 (2007).
10. P. Hrma, M. J. Schweiger, C. J. Humrickhouse, J. A. Moody, R. M. Tate, T. T. Rainsdon, N. E. TeGrotenhuis, B. M. Arrigoni, J. Marcial, C. P. Rodriguez, and B. H. Tincher, "Effect of glass-batch makeup on the melting process," *Ceramics-Silikaty* **54**, 193-211 (2010).
11. R. Conradt, P. Suwannathada, and P. Pinkhaokham, "Local temperature distribution and primary melt formation in a melting batch heap," *Glastech. Ber.* **67**, 103 (1994).
12. A. H. Gerrard and I. H. Smith, "Laboratory techniques for studying foam formation and stability in glass melting," *Glastech. Ber.* **56K**, 13-18 (1983).

13. J. Kappel, R. Conradt, and H. Scholze, "Foaming behavior in glass melts." *Glastech. Ber.* **60**, 189-201 (1978).

14. M. J. Schweiger, P. Hrma, C. J. Humrickhouse, J. Marcial, B. J. Riley, and N. E. TeGrotenhuis, "Cluster formation of silica particles in glass batches during melting," *J. Non-Cryst. Solids* **356** [25-27] 1359–1367 (2010).

15. S. Henager, H., P. Hrma, K.J. Swearingen, M. J. Schweiger, J. Marcial, and N. E. TeGrotenhuis, "Conversion of batch to molten glass, I: Volume expansion," accepted in *J. Non-Cryst. Solids.*

16. P. Hrma, K. J. Swearingen, S. H. Henager, M. J. Schweiger, J. Marcial, N. E. TeGrotenhuis, Conversion of batch to molten glass, II: Dissolution of quartz particles, *J. Non-Cryst. Solids*. **357**, 820-828 (2011).

17. P. Hrma, B. M. Arrigoni, M. J. Schweiger, "Viscosity of many-component glasses", *J. Non-Cryst. Solids* **355** [14-15] 891–902 (2009).

18. J. G. Darab, E. M. Meiers, and P. A. Smith, "Behavior of Simulated Hanford Slurries During Conversion to Glass," *Mat. Res. Soc. Proc.* **556**, 215-222 (1999).

19. P.A. Smith, J.D. Vienna, and P. Hrma, "The Effects of Melting Reactions on Laboratory-Scale Waste Vitrification," *J. Mat. Res*., **10** [8] 2137-2149 (1995)

20. P. Hrma, J. Matyáš, and D.-S. Kim, "The Chemistry and Physics of Melter Cold Cap," *9th Biennial Int. Conf. On Nucl. And Hazardous Waste Management, Spectrum '02*, American Nuclear Society, CD-ROM (2002).

21. H. D. Schreiber, C. W. Schreiber, M. W. Riethmiller, J. S. Downey, "The Effect of Temperature on the Redox Constraints for the Processing of High-Level Nuclear Waste into a Glass Waste Form," *Materials Research Society Symposium Proceeding*, **176**, 419–426 (1990).

22. J. A. Duffy, F. G. K. Baucke, "Effect of glass composition and basicity on reduction of metal ions to the metallic state in melts," *Phys. Chem. Glasses* **38** [1] 25-26 (1997).

Figure captions

Figure 1. Mass-loss rates and mass loss per unit mass of glass (inset) of batches as functions of temperature.

Figure 2. Photographic images of pressed pellets during heating.

Figure 3. Normalized profile areas of pellets versus temperature.

Figure 4. Fractions of undissolved quartz and corundum versus temperature. The coefficients of determination (R^2) and the standard errors (s) are: $R^2 = 0.977$ and $s = 0.062$ for quartz in batch with corundum; $R^2 = 0.996$ and $s = 0.029$ for quartz in batch with gibbsite; $R^2 = 0.991$ and $s = 0.047$ for quartz in batch with boehmite; $R^2 = 0.983$ and $s = 0.067$ for corundum.

Figure 5. Dissolution rate of quartz and corundum versus temperature.

Figure 6. Crystalline fractions of aluminum-containing crystalline phases in batches.

Figure 7. SEM micrographs and EDS of batches with corundum at 600°C (A) and 700°C (B), and with gibbsite at 700°C (C).

Figure 8. Optical images of thin sections of melts from corundum- and gibbsite-containing batches heated in Pt crucibles at 5°C/min.

Figure 9. Optical micrograph of a melt heated to 1200°C at 5°C/min in a Pt crucible. The streaks trace circulation flow typical for the meniscus area on the left. Bright spots at the bottom are high-silica inhomogeneities stuck to the Pt surface. A rising bubble dragging the melt in its wake, while stretching and thinning the inhomogeneities, as can be seen on the right.

Table 1. Steady state rate of melting in a small electric melter equipped with bubbling [1]

Al source	W[(a)] Fraction	Rate of melting $g/m^2/s$	
		1150°C	1200°C
Al_2O_3	0.436	8	15
$Al(OH)_3$	0.436	11	16
$Al(OH)_3$	0.450	11	17
AlO(OH)	0.450	14	19

(a) W is the mass fraction of glass components from the waste

Table 2. Composition of batch with gibbsite in g per g of glass.

Compound	Fraction
$Al(OH)_3$	0.368
SiO_2	0.305
H_3BO_3	0.270
NaOH	0.099
Li_2CO_3	0.088
$Fe(OH)_3$	0.074
CaO	0.061
NaF	0.015
$Bi(OH)_3$	0.013
$Fe(H_2PO_2)_3$	0.012
Na_2CrO_4	0.011
$Zr(OH)_4 \cdot H_2O$	0.006
$NiCO_3$	0.006
$Pb(NO_3)_2$	0.006
Na_2SO_4	0.004
$Zn(NO_3)_2 \cdot 4H_2O$	0.003
KNO_3	0.003
$NaNO_2$	0.003
$Mg(OH)_2$	0.002
$Na_2C_2O_4$	0.001
Total	1.350

Table 3. Batch-to-glass ratios.

	Batch-to-glass mass ratio		Difference
Al source	As batched[(a)]	Dried[(b)]	
Al_2O_3	1.223	1.150	0.073
$Al(OH)_3$	1.350	1.272	0.078
AlO(OH)	1.260	1.170	0.090

(a) Mix of batch chemicals as weighed.
(b) As determined by TGA.

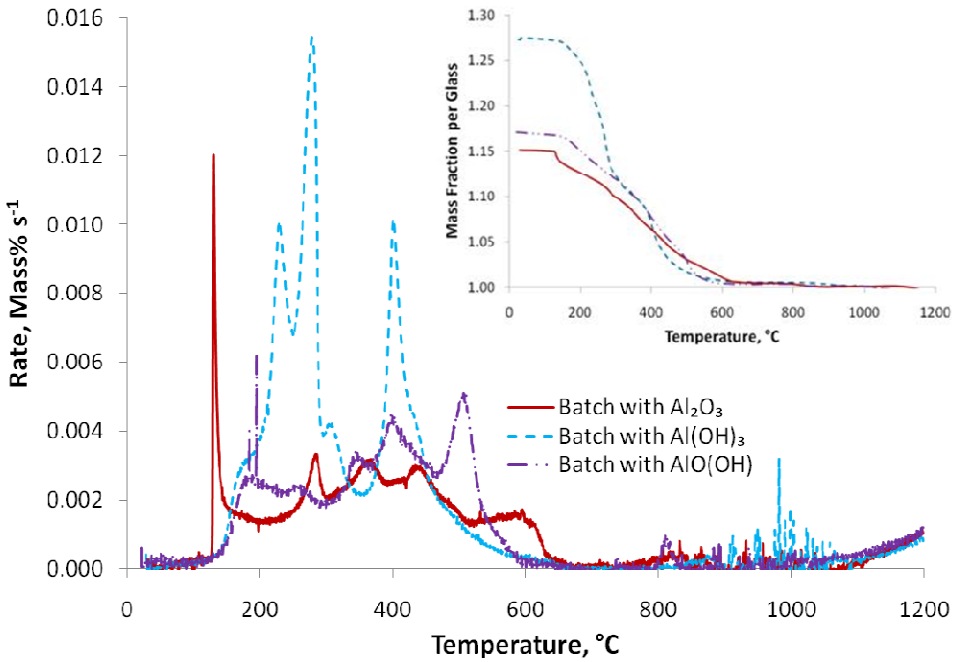
0.016
0.014
0.012
0.010
0.008
0.006
0.004
0.002
0.000
Rate, Mass% s-1
0
200
400
600
800
1000
1200
Temperature, °C
Batch with Al2O3
Batch with Al(OH)3
Batch with AlO(OH)
1.30
1.25
1.20
1.15
1.10
1.05
1.00
Mass Fraction per Glass
0
200
400
600
800
1000
1200
Temperature, °C

Figure 1.

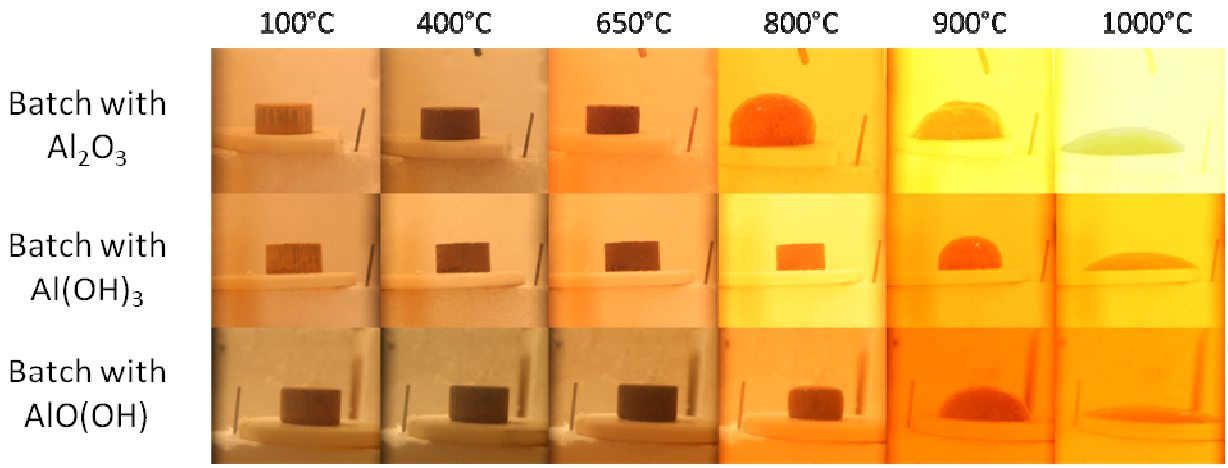
100°C
400°C
650°C
800°C
900°C
1000°C
Batch with Al_2O_3
Batch with $Al(OH)_3$
Batch with AlO(OH)

Figure 2.

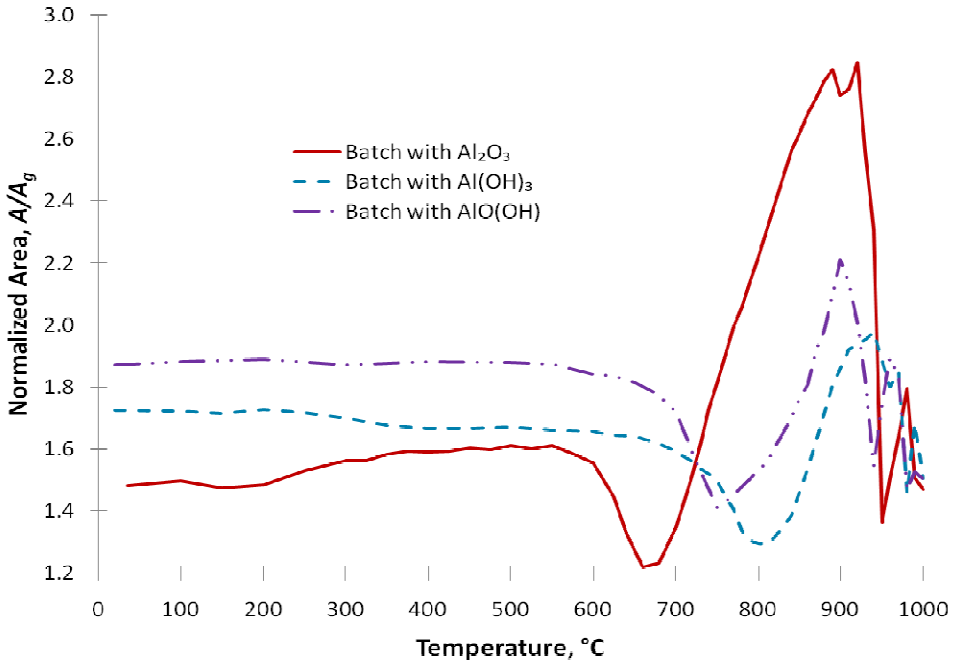
3.0
2.8
2.6
2.4
2.2
2.0
1.8
1.6
1.4
1.2
Normalized Area, A/Ag
Batch with Al2O3
Batch with Al(OH)3
Batch with AlO(OH)
0
100
200
300
400
500
600
700
800
900
1000
Temperature, °C

Figure 3.

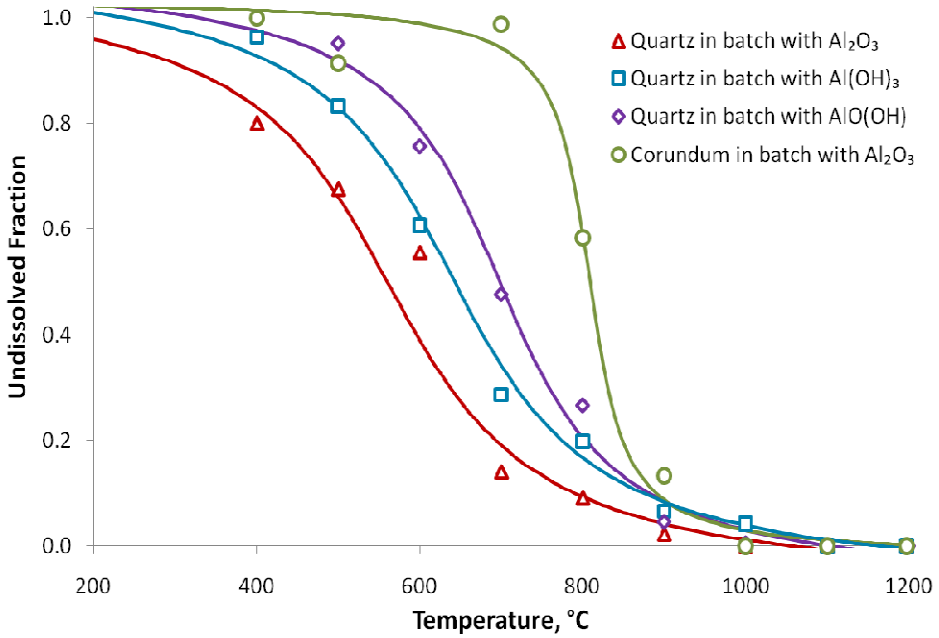
1.0
0.8
0.6
0.4
0.2
0.0
Undissolved Fraction
200
400
600
800
1000
1200
Temperature, °C
Quartz in batch with Al_2O_3
Quartz in batch with $Al(OH)_3$
Quartz in batch with AlO(OH)
Corundum in batch with Al_2O_3

Figure 4.

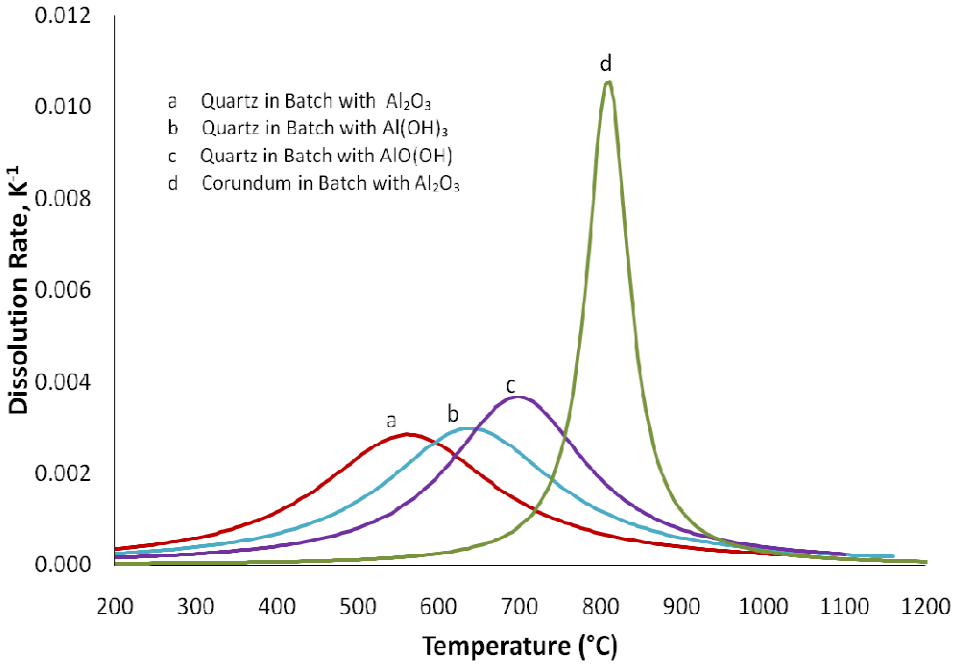
0.012
0.010
0.008
0.006
0.004
0.002
0.000
Dissolution Rate, K-1
a Quartz in Batch with Al2O3
b Quartz in Batch with Al(OH)3
c Quartz in Batch with AlO(OH)
d Corundum in Batch with Al2O3
a
b
c
d
200
300
400
500
600
700
800
900
1000
1100
1200
Temperature (°C)

Figure 5.

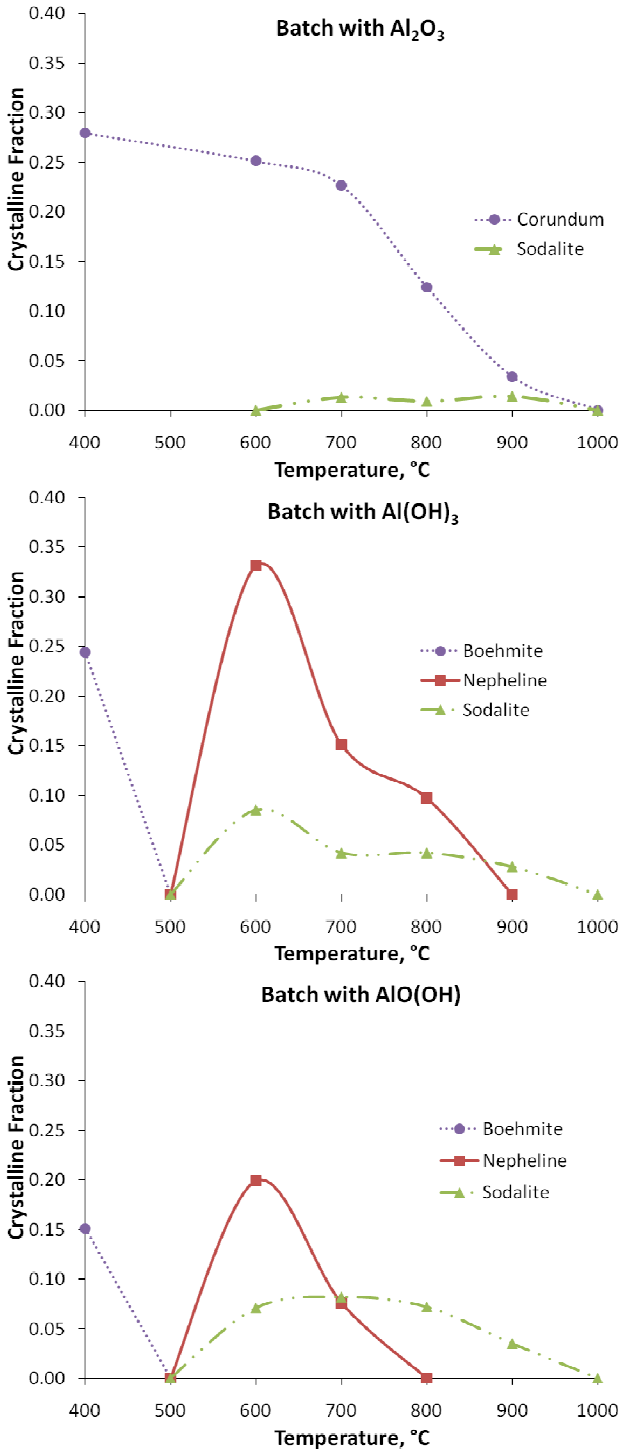
Batch with Al_2O_3
Crystalline Fraction
0.40
0.35
0.30
0.25
0.20
0.15
0.10
0.05
0.00
400
500
600
700
800
900
1000
Temperature, °C
Corundum
Sodalite
Batch with $Al(OH)_3$
Crystalline Fraction
Temperature, °C
Boehmite
Nepheline
Sodalite
Batch with AlO(OH)
Crystalline Fraction
Temperature, °C
Boehmite
Nepheline
Sodalite

Figure 6.

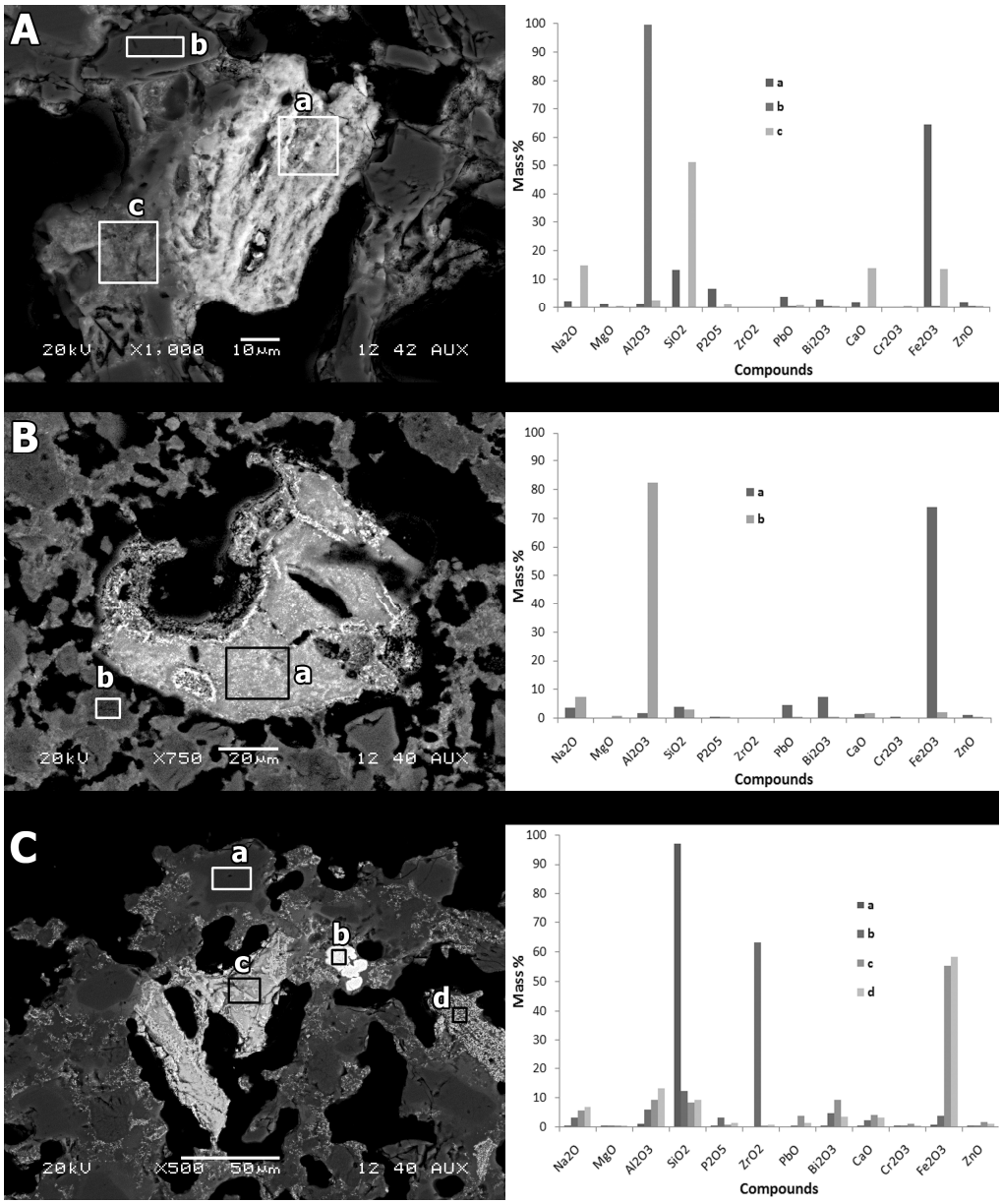
A
b
a
c
20kV X1,000 10µm 12 42 AUX
Mass %
Compounds
Na2O
MgO
Al2O3
SiO2
P2O5
ZrO2
PbO
Bi2O3
CaO
Cr2O3
Fe2O3
ZnO
a
b
c
B
b
a
20kV X750 20µm 12 40 AUX
C
a
b
c
d
20kV X500 50µm 12 40 AUX

Figure 7.

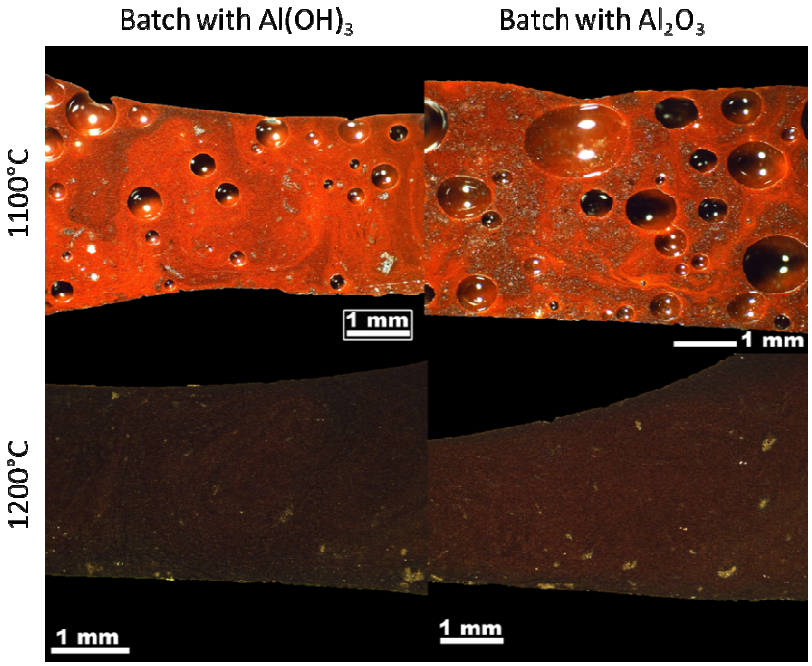
Batch with Al(OH)3
Batch with Al2O3
1100°C
1200°C
1 mm
1 mm
1 mm
1 mm

Figure 8.

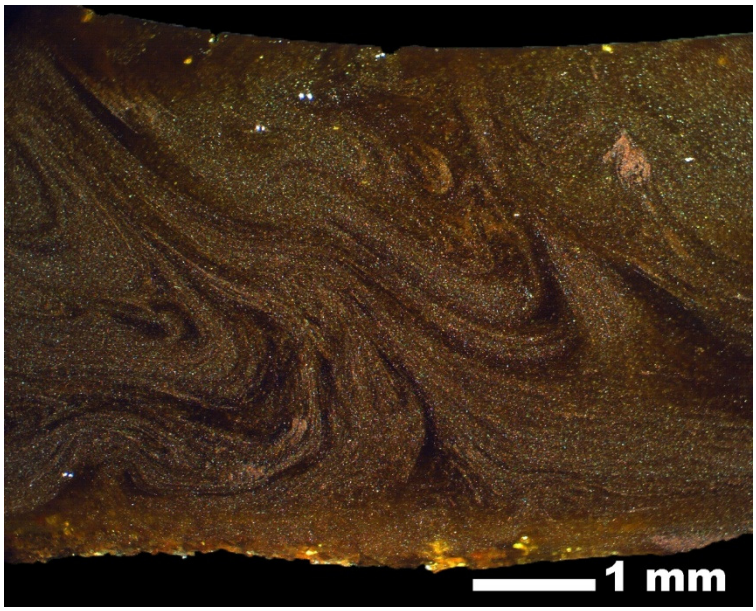

Figure 9.